Solute transport with Michaelis-Menten kinetics for *in vitro* cell culture

Lauren Hyndman[1], Sean McKee[2], and Sean McGinty[1*]

[1]Division of Biomedical Engineering, University of Glasgow, Glasgow G12 8QQ, UK.

[2]Department of Mathematics and Statistics, University of Strathclyde, Glasgow G1 1XQ, UK.

[*]Corresponding author. Tel.: +44 141 3308588. Email address: sean.mcginty@glasgow.ac.uk.

Abstract

A traditional method of *in vitro* cell culture involves a monolayer of cells at the base of a petri dish filled with culture medium. While the primary role of the culture medium is to supply nutrients to the cells, drug or other solutes may be added, depending on the purpose of the experiment. Metabolism by cells of oxygen, nutrients and drug is typically governed by Michaelis-Menten (M-M) kinetics. In this paper, a mathematical model of solute transport with M-M kinetics is developed. Upon non-dimensionalisation, the reaction/diffusion system is re-characterised in terms of Volterra integral equations, where a parameter β, the ratio of the initial solute concentration to the M-M constant, proves important: $\beta \ll 1$ is relevant to drug metabolism for the liver, whereas $\beta \gg 1$ is more appropriate in the case of oxygen metabolism. Regular perturbation expansions for both cases are obtained. A small time expansion and steady-state solution are also presented. All results are compared against the numerical solution of the Volterra integral equations, and excellent agreement is found. The utility of the model and analytical solutions are discussed in the context of assisting experimental researchers to better understand the environment within *in vitro* cell culture experiments.

Keywords

In vitro cell culture, Michaelis-Menten kinetics, Laplace transforms, Volterra integral equations, regular perturbation expansions, small t expansion.

1 Introduction

The practice of cultivating cells under controlled conditions outwith a living organism, known as *in vitro* cell culture, has been employed for over a century across a wide range of applications. For example, *in vitro* cell cultures form a critical part of the drug development pathway, and provide a platform for investigation of disease initiation and progression. A traditional method of *in vitro* cell culture involves culturing a monolayer of cells at the base of a petri dish filled with culture medium, whose primary role is to supply nutrients to the cells. Despite significant advances in recent years to increase the physiological relevance of *in vitro* cell culture, for example the development of perfusion bioreactors and the incorporation of three-dimensional cell structures, this traditional method is still widely adopted today, remaining a popular choice due to its ease of use, reproducibility and low-cost [1, 2]. Within the typical static *in vitro* environment, conditions must be optimal to ensure the growth and/or survival of a healthy cell culture; for example, cells should receive a sufficient supply of oxygen (O_2) and nutrients, and in the case of drug testing, optimal dosage must be determined. Thus, there is scope for mathematical modelling to provide useful information that can inform, and improve, experimental design. Mathematical models of solute transport and metabolism can be used to tailor the set-up of an experiment such that the ideal O_2, nutrient and/or drug concentrations are achieved and, furthermore, can provide insight into issues such as how often the culture medium should be replenished in order to maintain certain thresholds over time.

There are many mechanisms by which the interaction between the solute of interest and the cells can be described; in this paper, Michaelis-Menten (M-M) kinetics are used to characterise solute metabolism, a common approach in the literature [3], particularly when the solute of interest is O_2 or a drug such as paracetamol (routinely used for *in vitro* toxicity testing [4]). Previously, diffusion and M-M kinetics have been used to describe the transport and metabolism of O_2 within set-ups representative of standard static *in vitro* experiments. For example, Demol et al. [5] and Zhao et al. [6] developed mathematical models and used numerical methods to estimate the O_2 concentrations within cell-seeded hydrogels and cell-seeded scaffolds, respectively. For a monolayer of cells at the base of a petri dish, a computational model presented by Przekwas et al. [7] was used to predict O_2 concentrations within the cell layer for various depths of culture medium. Considering a similar experimental set-up but with a focus on cell growth, a mathematical model developed by Burova et al. [8] was solved numerically and parameterised by comparing experimental data with simulated results. Finally, in a study by Yarmush et al. [9], the governing equations were solved analytically to provide the O_2 concentration at the surface of a layer of cells at the base of a petri dish. However, only the steady-state solution was provided.

With the exception of [9], the aforementioned studies were computational in nature and there-

fore produced purely numerical results: this can be highly useful if the goal is to predict the environment within a specific set-up, and the visual representations obtained from numerical solutions are often appealing and easy to interpret. However, such results provide little information on the form of the mathematical solution and its dependence on the underlying model parameters. Therefore, it is difficult to generalise the results in the event of any changes to experimental design; instead, it would be necessary to re-run a computational model with updated input parameters, which can be time-consuming. On the contrary, an analytical approach provides an exact solution to a set of governing equations that clearly highlights the interplay between the various model parameters, and that can readily be updated to account for different cell culture conditions.

In this paper, we present a mathematical model of solute transport within a petri dish, including metabolism of solute by a monolayer of cells. A series of approximate analytical solutions are derived and excellent agreement is found upon comparison with numerical solutions. The key advantage of the analytical solutions is that they clearly highlight the dependence of the cell surface solute concentration on the various parameters of the model, enabling the more efficient design of experiments. The remainder of the paper is organised as follows. In section 2, we formulate the mathematical model before performing non-dimensionalisation, enabling us to express the model in terms of three key non-dimensional parameters. We then provide motivation for the consideration of one of these parameters (β, the ratio of initial solute concentration to the M-M constant) being either small or large. In section 3, we re-characterise the model using two methods. First, Laplace transforms is used to derive Volterra integral equations for (i) the solute concentration at any depth within the petri dish, and (ii) the solute concentration at the cell surface. We consider the special case of a zero flux boundary condition at the fluid/air interface and show that a different Volterra integral equation is required, due to a subtlety in the inversion of the solution in Laplace transform space. Secondly, a result from Cannon [10] is used to derive two coupled Volterra integral equations for (i) the solute concentration at the fluid/air interface, and (ii) the solute concentration at the cell surface. In section 4, we derive a regular perturbation solution for the cases of small β and large β, then in section 5 we derive an approximate solution for small time and present the steady-state solution. In section 6, we provide results comparing the approximate solutions with the numerical solutions of the Volterra integral equations, before considering two case studies involving O_2 and drug metabolism, respectively. Finally, in section 7, we discuss how the solutions may be exploited to provide useful information when configuring *in vitro* cell culture experiments.

2 The mathematical model

Consider a typical static *in vitro* experimental set-up, where a single layer of cells line the base of a petri dish of radius R that is filled to a depth d with fluid containing solute (see Fig. 2.1). Given

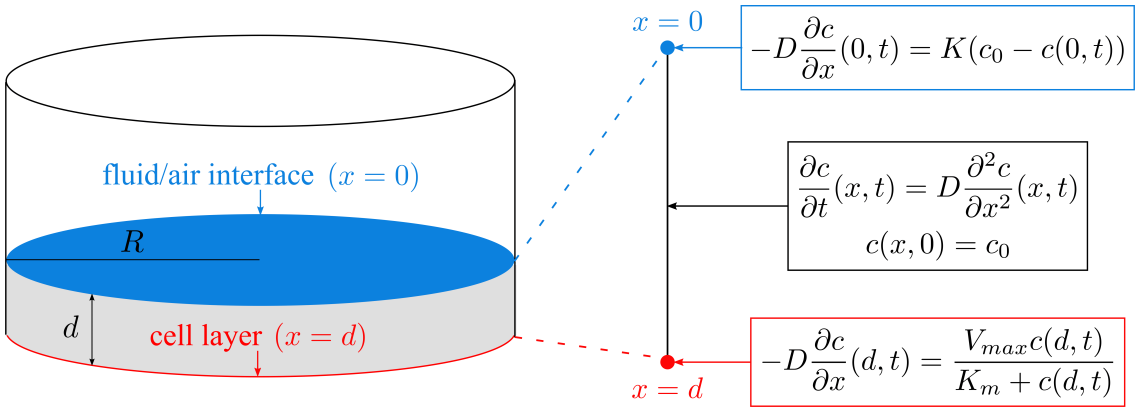

Figure 2.1: Schematic drawing (not to scale) illustrating a typical static *in vitro* experimental set-up (left) and the 1D domain over which the governing equations are solved (right).

the simple geometry of a petri dish with $d \ll R$ (see Table 2.1 for typical values), coupled with the form of the initial and boundary conditions under consideration, it is sufficient to describe a reaction-diffusion problem in the vertical direction. Here, we choose x and t as the spatial and temporal co-ordinates, respectively.

We describe transport of the solute through the fluid via diffusion, i.e.

$$\frac{\partial c}{\partial t}(x,t) = D\frac{\partial^2 c}{\partial x^2}(x,t), \quad 0 < x < d, \quad t > 0, \tag{2.1}$$

where $c(x,t)$ (mol m^{-3}) is the solute concentration and D (m^2 s^{-1}) is the constant isotropic diffusion coefficient. Initially, the concentration of the solute within the fluid is assumed to be constant:

$$c(x,0) = c_0, \quad 0 < x < d. \tag{2.2}$$

In general, the flux of solute at the fluid/air interface is proportional to the difference between the solute concentration in the air and at the interface, i.e.

$$-D\frac{\partial c}{\partial x}(0,t) = K(c_0 - c(0,t)), \quad t > 0, \tag{2.3}$$

Diameter of dish (mm)	***Recommended volume (mL)***	***Depth of fluid (mm)***
35	1.8 - 2.7	1.9 - 2.8
60	4.2 - 6.3	1.5 - 2.2
100	11.0 - 16.5	1.4 - 2.1
150	30.4 - 45.6	1.7 - 2.6

Table 2.1: Diameter ($2R$) of Corning culture dishes and recommended volume of fluid taken from [11], with the associated fluid depth (d) calculated using $V = \pi R^2 d$.

where K ($\mathrm{m\ s^{-1}}$) is the mass transfer coefficient, and the solute concentration in the air is given by c_0 since Henry's law dictates that, initially, the concentration of solute in the air and the fluid must be equal. It is noted that a special case will be considered for solutes that cannot cross the fluid/air interface (such as drug) where we set $K = 0$ and consider zero flux across this boundary.

At the base of the petri dish, it is assumed that the cell population is maintained at a fixed number. We further assume that the thickness of the cell layer is negligible in comparison to the depth of the fluid, so we can use a flux boundary condition to represent the interaction between the solute and the cells. Here, M-M kinetics describe solute metabolism:

$$-D\frac{\partial c}{\partial x}(d,t) = \frac{V_{max}c(d,t)}{K_m + c(d,t)}, \quad t > 0, \tag{2.4}$$

where V_{max} ($\mathrm{mol\ m^{-2}\ s^{-1}}$) is the maximum metabolic rate and K_m ($\mathrm{mol\ m^{-3}}$) is the M-M constant, representing the solute concentration for which the metabolic rate is half maximal.

The governing equations (2.1) - (2.4) are non-dimensionalised using the scalings

$$c = c_0 c', \quad t = \frac{d^2}{D}t', \quad x = dx',$$

and so, dropping the primes for clarity, the non-dimensional model is given by

$$\frac{\partial c}{\partial t}(x,t) = \frac{\partial^2 c}{\partial x^2}(x,t), \quad 0 < x < 1, \quad t > 0, \tag{2.5}$$

$$c(x,0) = 1, \quad 0 < x < 1, \tag{2.6}$$

$$\frac{\partial c}{\partial x}(0,t) = -\mu\big[1 - c(0,t)\big], \quad t > 0, \tag{2.7}$$

$$\frac{\partial c}{\partial x}(1,t) = -\frac{\alpha c(1,t)}{1 + \beta c(1,t)}, \quad t > 0, \tag{2.8}$$

where the resulting non-dimensional parameters are defined as follows:

$$\mu = \frac{Kd}{D}, \quad \alpha = \frac{V_{max}d}{DK_m}, \quad \beta = \frac{c_0}{K_m}.$$

2.1 Motivation for the consideration of small β and large β

Clearly, the values of the three non-dimensional parameters μ, α and β will vary depending on the experimental configuration, as well as the solute and cell type under consideration. Whilst it is clear that the two extremes of μ (0 and ∞, representing zero flux of solute and a constant source of solute at the fluid/air interface, respectively) are both possible, one must turn to the experimental literature in order to estimate a reasonable physiological range of α and β. We have uncovered

that β is typically large for the case of O_2 metabolism, and is typically relatively small when drugs primarily metabolised by the liver are considered (see Table 2.2). This provides sufficient motivation to explore approximate solutions that are valid for small β and large β.

Parameter	***Description***	***Case 1: O_2 metabolism***	***Case 2: Drug metabolism***
d	Depth of fluid	4.50×10^{-3} m	4.50×10^{-3} m
D	Diffusion coefficient	1.91×10^{-9} m^2 s^{-1}	7.50×10^{-10} m^2 s^{-1}
c_0	Initial concentration	2.18×10^{-1} mol m^{-3}	1.00×10^{-1} mol m^{-3}
V_{max}	Maximum metabolic rate	1.19×10^{-8} mol m^{-2} s^{-1}	3.49×10^{-8} mol m^{-2} s^{-1}
K_m	Michaelis-Menten constant	3.33×10^{-3} mol m^{-3}	1.40×10^{-1} mol m^{-3}
μ	Kd/D	∞	0
α	$V_{max}d/DK_m$	8.42	1.50
β	c_0/K_m	65.47	0.71

Table 2.2: Dimensional and non-dimensional parameter values relating to O_2 (case 1) and drugs primarily metabolised in the liver (case 2). **Case 1**: Values taken from [8]. To obtain V_{max} in appropriate units, the provided value (2.55×10^{-17} mol cell^{-1} s^{-1}) was multiplied by the cell density (4.66×10^8 cells m^{-2}). The value of μ represents a constant source of O_2 at the fluid/air interface. **Case 2**: Values taken from [12] (with the exception of d [8]). To obtain V_{max} in appropriate units, the provided value (5.00×10^{-3} mol m^{-3} s^{-1}) was multiplied by the height of the cell layer (6.99×10^{-6} m), calculated by multiplying the cell density (4.66×10^8 cells m^{-2} [8]) by the volume of a single cell (1.50×10^{-14} m^3 [13]). The value of μ reflects zero flux of drug at the fluid/air interface.

3 Model re-characterisation

The non-dimensional model (2.5) - (2.8) permits re-characterisation both as a single nonlinear Volterra integral equation, and also as a system of two nonlinear singular Volterra integral equations. This section will be concerned with their derivation.

3.1 Formulation 1: a single integral equation

Here, Laplace transforms are used to derive a Volterra integral equation that describes the concentration of solute at the cell surface, $c(1,t)$. This formulation will be used to obtain perturbation expansions that are valid for small and large β.

By the method of Laplace transforms, the solution of (2.5) subject to (2.6) - (2.7) is

$$\bar{c}(x,s) = A(s)\cosh(\sqrt{s}x) + \frac{\mu A(s)}{\sqrt{s}}\sinh(\sqrt{s}x) + \frac{1}{s},$$

where

$$\bar{c}(x,s) = \int_0^\infty e^{-st}c(x,t)\,dt.$$

Differentiating with respect to x, applying (2.8) and re-arranging allows one to obtain the following expression for $A(s)$:

$$A(s) = -\frac{1}{\sqrt{s}\sinh(\sqrt{s}) + \mu\cosh(\sqrt{s})}\mathcal{L}\left\{\frac{\alpha c(1,t)}{1+\beta c(1,t)}\right\},$$

so it follows that the solution in Laplace transform space may be written as

$$\bar{c}(x,s) = \frac{1}{s} - \bar{k}(x,s)\mathcal{L}\left\{\frac{\alpha c(1,t)}{1+\beta c(1,t)}\right\}, \tag{3.1}$$

where

$$\bar{k}(x,s) = \frac{\sqrt{s}\cosh(\sqrt{s}x) + \mu\sinh(\sqrt{s}x)}{\sqrt{s}\big[\sqrt{s}\sinh(\sqrt{s}) + \mu\cosh(\sqrt{s})\big]}.$$

By taking the inverse Laplace transform of (3.1) and employing the convolution theorem, the following relationship is obtained:

$$c(x,t) = 1 - \alpha\int_0^t k(x,t-\tau)\frac{c(1,\tau)}{1+\beta c(1,\tau)}\,d\tau, \tag{3.2}$$

where

$$k(x,t) = \mathcal{L}^{-1}\left\{\frac{\sqrt{s}\cosh(\sqrt{s}x) + \mu\sinh(\sqrt{s}x)}{\sqrt{s}\big[\sqrt{s}\sinh(\sqrt{s}) + \mu\cosh(\sqrt{s})\big]}\right\}.$$

Given that no branch points exist (as can be observed through consideration of Taylor series expansions of $\sinh$ and $\cosh$), the residue theorem may be used to evaluate this inverse Laplace transform. It is noted that $s = 0$ is a removable singularity, so the poles are given by

$$\sqrt{s}\sinh(\sqrt{s}) + \mu\cosh(\sqrt{s}) = 0,$$

and, for convenience, setting $\sqrt{s} = i\gamma$ in this transcendental equation gives

$$\mu\cos(\gamma) - \gamma\sin(\gamma) = 0. \tag{3.3}$$

Thus, there are infinitely many simple poles at $s_n = -\gamma_n^2$ for $n \in \mathbb{N}$, where γ_n are the roots of (3.3). The residue at $s = s_n$ is calculated by re-writing the limit as $s \to s_n$ as the product of two limits, the first of which may be evaluated by making use of L'Hôpital's rule, and then substituting $\sqrt{s_n} = i\gamma_n$:

$$\begin{aligned}\operatorname*{Res}_{s=s_n} &= \lim_{s\to s_n}\left\{\frac{\sqrt{s}\cosh(\sqrt{s}x)+\mu\sinh(\sqrt{s}x)}{\sqrt{s}\big[\sqrt{s}\sinh(\sqrt{s})+\mu\cosh(\sqrt{s})\big]}(s-s_n)e^{st}\right\}\\ &= \lim_{s\to s_n}\left\{\frac{s-s_n}{\sqrt{s}\sinh(\sqrt{s})+\mu\cosh(\sqrt{s})}\right\}\times\\ &\quad \lim_{s\to s_n}\left\{\frac{\big[\sqrt{s}\cosh(\sqrt{s}x)+\mu\sinh(\sqrt{s}x)\big]}{\sqrt{s}}e^{st}\right\}\\ &= \frac{2\big[\gamma_n\cos(\gamma_n x)+\mu\sin(\gamma_n x)\big]}{\gamma_n\cos(\gamma_n)+(\mu+1)\sin(\gamma_n)}e^{-\gamma_n^2 t}.\end{aligned}$$

Then, applying the residue theorem gives

$$k(x,t)=2\sum_{n=1}^{\infty}\frac{\gamma_n\cos(\gamma_n x)+\mu\sin(\gamma_n x)}{\gamma_n\cos(\gamma_n)+(\mu+1)\sin(\gamma_n)}e^{-\gamma_n^2 t}. \tag{3.4}$$

When $x=1$, (3.2) reduces to a second kind nonlinear Volterra integral equation, given by

$$c(1,t)=1-\alpha\int_0^t k(1,t-\tau)\frac{c(1,\tau)}{1+\beta c(1,\tau)}\,d\tau, \tag{3.5}$$

where

$$k(1,t-\tau)=2\sum_{n=1}^{\infty}\frac{\gamma_n\cos(\gamma_n)+\mu\sin(\gamma_n)}{\gamma_n\cos(\gamma_n)+(\mu+1)\sin(\gamma_n)}e^{-\gamma_n^2(t-\tau)},$$

i.e.

$$c(1,t)=1-2\alpha\int_0^t\sum_{n=1}^{\infty}\frac{\gamma_n\cos(\gamma_n)+\mu\sin(\gamma_n)}{\gamma_n\cos(\gamma_n)+(\mu+1)\sin(\gamma_n)}e^{-\gamma_n^2(t-\tau)}\frac{c(1,\tau)}{1+\beta c(1,\tau)}\,d\tau.$$

The solution of (3.5) then allows one, in principle at least, to evaluate $c(x,t)$ for all $x\in[0,1]$ using (3.2).

An integral equation can also be obtained for the special case when $\mu=0$, applicable to solutes such as drug that cannot cross the fluid/air interface. At first glance, it might be supposed that $\mu=0$ is simply substituted into (3.4); however, this does not give rise to the correct expression because in this case, $s=0$ is not a removable singularity. Therefore, the residue at this simple pole provides a non-zero contribution:

$$\operatorname*{Res}_{s=0}=\lim_{s\to 0}\left\{\left.\frac{\sqrt{s}\cosh(\sqrt{s}x)+\mu\sinh(\sqrt{s}x)}{\sqrt{s}\big[\sqrt{s}\sinh(\sqrt{s})+\mu\cosh(\sqrt{s})\big]}\right|_{\mu=0}se^{st}\right\}=1.$$

Thus, when $\mu=0$, the second kind nonlinear Volterra integral equation describing the solute concentration at $x=1$ is given by

$$c(1,t)=1-\alpha\int_0^t k_0(1,t-\tau)\frac{c(1,\tau)}{1+\beta c(1,\tau)}\,d\tau, \tag{3.6}$$

where

$$k_0(1,t) = 1 + 2\sum_{n=1}^{\infty} \frac{\gamma_n \cos(\gamma_n)}{\gamma_n \cos(\gamma_n) + \sin(\gamma_n)} e^{-\gamma_n^2 t}.$$

Note that when $\mu = 0$, (3.3) reduces to $\sin(\gamma) = 0$, i.e. $\gamma_n = n\pi$ for $n \in \mathbb{N}$. Thus, $k_0(1,t)$ may be re-written as

$$k_0(1,t) = 1 + 2\sum_{n=1}^{\infty} e^{-n^2\pi^2 t}.$$

3.2 Formulation 2: a system of integral equations

Here, the following result from Cannon [10] (see Corollary 7.3.2) is used to derive two coupled Volterra integral equations that describe the concentration of solute at the fluid/air interface, $c(0,t)$, and the cell surface, $c(1,t)$. This formulation allows for characterisation of the behaviour of the solution at small times.

Lemma 1. *For piecewise-continuous f, and continuous F and G, the problem*

$$\begin{aligned}
\frac{\partial u}{\partial t}(x,t) &= \frac{\partial^2 u}{\partial x^2}(x,t), \quad 0 < x < 1, \quad t > 0, \\
u(x,0) &= f(x), \quad 0 < x < 1, \\
\frac{\partial u}{\partial x}(0,t) &= F(t, u(0,t)), \quad t > 0, \\
\frac{\partial u}{\partial x}(1,t) &= G(t, u(1,t)), \quad t > 0,
\end{aligned}$$

has a unique solution if and only if the function $u(x,t)$ can be expressed as

$$u(x,t) = w(x,t) - 2\int_0^t \theta(x, t-\tau) F(\tau, \phi_1(\tau))\, d\tau + 2\int_0^t \theta(x-1, t-\tau) G(\tau, \phi_2(\tau))\, d\tau,$$

where

$$w(x,t) = \int_0^1 \big[\theta(x-\xi, t) + \theta(x+\xi, t)\big] f(\xi)\, d\xi,$$

and

$$\theta(x,t) = \frac{1}{\sqrt{4\pi t}} \sum_{n=-\infty}^{\infty} e^{-(x+2n)^2/4t},$$

and $\phi_1(t)$, $\phi_2(t)$ are piecewise-continuous functions uniquely satisfying the system of Volterra integral equations given by

$$\phi_1(t) = w(0,t) - 2\int_0^t \theta(0,t-\tau)F(\tau,\phi_1(\tau))\,d\tau + 2\int_0^t \theta(-1,t-\tau)G(\tau,\phi_2(\tau))\,d\tau,$$
$$\phi_2(t) = w(1,t) - 2\int_0^t \theta(1,t-\tau)F(\tau,\phi_1(\tau))\,d\tau + 2\int_0^t \theta(0,t-\tau)G(\tau,\phi_2(\tau))\,d\tau.$$

From the governing equations (2.5) - (2.8), it is observed that

$$\begin{aligned} f(x) &= 1, \\ \phi_1(t) &= c(0,t), \\ \phi_2(t) &= c(1,t), \\ F(t,c(0,t)) &= -\mu(1-c(0,t)), \\ G(t,c(1,t)) &= -\frac{\alpha c(1,t)}{1+\beta c(1,t)}. \end{aligned}$$

Furthermore, we note that

$$\kappa_1 = 2\theta(0,t) = \frac{1}{\sqrt{\pi t}}\left(1 + 2\sum_{n=1}^{\infty} e^{-n^2/t}\right), \tag{3.7}$$
$$\kappa_2 = \theta(\pm 1,t) = \frac{1}{\sqrt{\pi t}}\sum_{n=1}^{\infty} e^{-(2n-1)^2/4t}. \tag{3.8}$$

Finally, it may readily be shown that

$$w(x,t) = \int_0^1 \big[\theta(x-\xi,t) + \theta(x+\xi,t)\big]\,d\xi = 1,$$

for all $x \in [0,1]$. Thus, from Lemma 1, a re-characterisation of the original reaction-diffusion problem may be obtained in terms of two coupled Volterra integral equations:

$$c(0,t) = 1 + \mu\int_0^t \kappa_1(t-\tau)\big[1-c(0,\tau)\big]\,d\tau - 2\alpha\int_0^t \kappa_2(t-\tau)\frac{c(1,\tau)}{1+\beta c(1,\tau)}\,d\tau, \tag{3.9}$$
$$c(1,t) = 1 + 2\mu\int_0^t \kappa_2(t-\tau)\big[1-c(0,\tau)\big]\,d\tau - \alpha\int_0^t \kappa_1(t-\tau)\frac{c(1,\tau)}{1+\beta c(1,\tau)}\,d\tau. \tag{3.10}$$

4 Perturbation expansions

In this section, we use formulation 1 of the model re-characterisation, i.e. the Volterra integral equations (3.5) and (3.6), to derive approximate solutions that are valid for small and large β, as motivated in section 2.1. It is noted that, at leading order, the asymptotic limits of β allow for linearisation of the M-M kinetics. Thus, an alternative approach to obtaining approximate solutions

(to leading order) is to solve the linear PDE models directly: these solutions are provided in the supplementary information, and match the approximate solutions we derive in this section. In contrast to directly solving the linear PDE models, the approximate solutions we derive from the Volterra integral equations provide the solution at precisely the spatial location of interest, i.e. at the cell surface. Furthermore, higher order terms can be sought when using the Volterra integral equations as a starting point for the asymptotic analysis, thereby providing additional information and highlighting the relative importance of the model parameters.

4.1 Small β solution

Here, we derive a regular perturbation solution of (3.5) for the case where β is small. Let $\beta \to 0$ and consider

$$c(1,t) = c_0(1,t) + \beta c_1(1,t) + \mathcal{O}(\beta^2). \tag{4.1}$$

Substituting this expression into (3.5) and equating powers of β gives

$$c_0(1,t) = 1 - \alpha \int_0^t k(1,t-\tau) c_0(1,\tau)\, d\tau, \tag{4.2}$$

$$c_1(1,t) = -\alpha \int_0^t k(1,t-\tau)\big[c_1(1,\tau) - c_0(1,\tau)^2\big]\, d\tau. \tag{4.3}$$

First, we can obtain an analytical expression for $c_0(1,t)$ by solving (4.2). Taking Laplace transforms, using the convolution theorem and re-arranging yields

$$\bar{c}_0(1,s) = \frac{1}{s\big[1 + \alpha \bar{k}(1,s)\big]}.$$

Then, taking the inverse Laplace transform and applying the residue theorem gives

$$c_0(1,t) = \frac{\mu}{\alpha\mu + \alpha + \mu} + \sum_{n=1}^{\infty} \frac{2\big[\mu\cos(\lambda_n) - \lambda_n \sin(\lambda_n)\big] e^{-\lambda_n^2 t}}{(\alpha\mu + \alpha + \mu - \lambda_n^2)\cos(\lambda_n) - \lambda_n(2 + \alpha + \mu)\sin(\lambda_n)}, \tag{4.4}$$

where λ_n are the countably infinite roots of

$$(\alpha\mu - \lambda^2)\sin(\lambda) + \lambda(\alpha + \mu)\cos(\lambda) = 0. \tag{4.5}$$

Thus, from (4.1), the approximate solution when $\beta \to 0$ is given by

$$\begin{aligned} c(1,t) = {} & \frac{\mu}{\alpha\mu + \alpha + \mu} + \sum_{n=1}^{\infty} \frac{2\big[\mu\cos(\lambda_n) - \lambda_n \sin(\lambda_n)\big]}{(\alpha\mu + \alpha + \mu - \lambda_n^2)\cos(\lambda_n) - \lambda_n(2 + \alpha + \mu)\sin(\lambda_n)} e^{-\lambda_n^2 t} \\ & + \beta c_1(1,t) + \mathcal{O}(\beta^2). \end{aligned} \tag{4.6}$$

It is noted that, in principle, an analytical expression for $c_1(1,t)$ may be obtained by applying Laplace transforms to (4.3) after substitution of (4.4) for $c_0(1,\tau)$. However, in practice, we solve (4.3) numerically using the methods detailed in the supplementary information. For the special case when $\mu = 0$, the above analysis can be repeated using (3.6) to obtain

$$c(1,t) = \sum_{n=1}^{\infty} \frac{2\sin(\chi_n)}{\chi_n \cos(\chi_n) + (\alpha+1)\sin(\chi_n)} e^{-\chi_n^2 t} + \beta c_1(1,t) + \mathcal{O}(\beta^2). \tag{4.7}$$

where it is noted that χ_n are the roots of (4.5) with $\mu = 0$, i.e.

$$\chi \sin(\chi) - \alpha \cos(\chi) = 0.$$

4.2 Large β solution

Here, we derive a regular perturbation solution of (3.5) for the case where β is large. Let $\beta \to \infty$, set $\varepsilon = 1/\beta$ and consider

$$c(1,t) = c_0(1,t) + \varepsilon c_1(1,t) + \mathcal{O}(\varepsilon^2). \tag{4.8}$$

Substituting this expression into (3.5) and equating powers of ε gives

$$\begin{aligned} c_0(1,t) &= 1, \\ c_1(1,t) &= -\alpha \int_0^t k(1,t-\tau)\, d\tau, \\ c_2(1,t) &= \alpha \int_0^t k(1,t-\tau)\, d\tau = -c_1(1,t). \end{aligned} \tag{4.9}$$

We can obtain an analytical expression for $c_1(1,t)$ by direct integration of (4.9):

$$c_1(1,t) = -\alpha \sum_{n=1}^{\infty} \frac{2\big[\gamma_n \cos(\gamma_n) + \mu \sin(\gamma_n)\big]}{\gamma_n^2 \big[\gamma_n \cos(\gamma_n) + (\mu+1)\sin(\gamma_n)\big]} \left(1 - e^{-\gamma_n^2 t}\right).$$

Thus, from (4.8), the approximate solution when $\beta \to \infty$ is given by

$$c(1,t) = 1 - \frac{\alpha}{\beta}\left(1 - \frac{1}{\beta}\right) \sum_{n=1}^{\infty} \frac{2\big[\gamma_n \cos(\gamma_n) + \mu \sin(\gamma_n)\big]}{\gamma_n^2 \big[\gamma_n \cos(\gamma_n) + (\mu+1)\sin(\gamma_n)\big]} \left(1 - e^{-\gamma_n^2 t}\right) + \mathcal{O}(1/\beta^3). \tag{4.10}$$

For the special case when $\mu = 0$, the above analysis can be repeated using (3.6) to obtain

$$c(1,t) = 1 - \frac{\alpha}{\beta}\left(1 - \frac{1}{\beta}\right)\left(t + \frac{1}{3} - 2\sum_{n=1}^{\infty} \frac{1}{n^2\pi^2} e^{-n^2\pi^2 t}\right) + \mathcal{O}(1/\beta^3). \tag{4.11}$$

5 Small and large t solutions

In this section, we use formulation 2 of the model re-characterisation, i.e. the Volterra integral equations (3.9) and (3.10), to derive an approximate solution that is valid for small t. Experimentally, it is of interest to develop an understanding of the behaviour of the solution at early times: for example, if the solute is found to deplete rapidly at the beginning of the experiment, this could provide an indication that a higher initial concentration of solute is required to maintain a desired set of cell culture conditions. Further to this, the duration of experiments often outlasts the time taken for the system to reach equilibrium, so it is also of relevance to examine the steady-state solution; this is presented here.

5.1 Small t solution

In order to use (3.9) and (3.10) to derive an approximate solution for small t, it is necessary to examine the behaviour of κ_1 and κ_2 (given by (3.7) and (3.8), respectively) as $t \to 0$; we will do this using Riemann sums. First considering κ_1, it is clear from Fig. 5.1 that

$$\int_1^\infty e^{-x^2/t}\,dx < \sum_{n=1}^{\infty} e^{-n^2/t} < \int_0^\infty e^{-x^2/t}\,dx.$$

Evaluation of these integrals yields

$$\frac{\sqrt{\pi t}}{2}\operatorname{erfc}\left(\frac{1}{\sqrt{t}}\right) < \sum_{n=1}^{\infty} e^{-n^2/t} < \frac{\sqrt{\pi t}}{2},$$

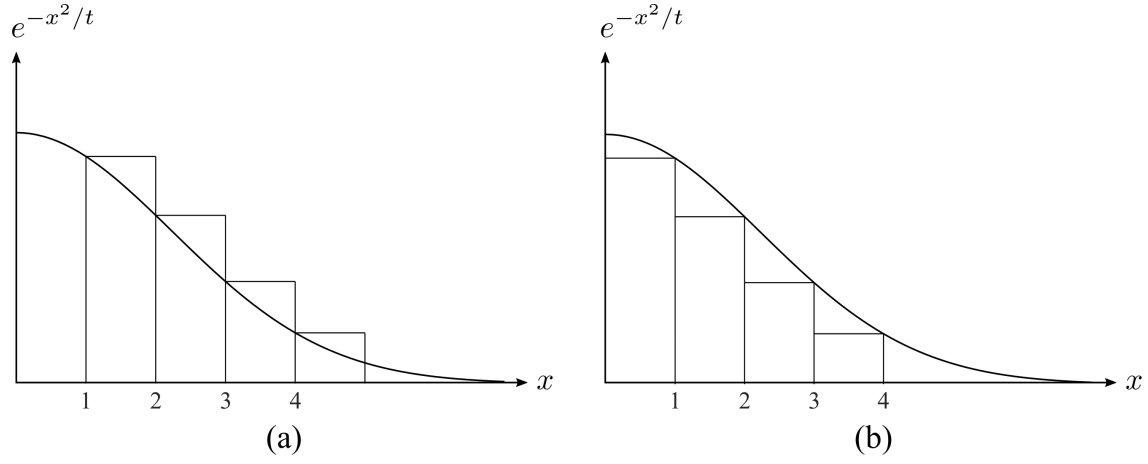

Figure 5.1: Schematic drawing illustrating the area under the curve $e^{-x^2/t}$ and an approximation to this area using (a) lower and (b) upper Riemann sums.

and from (3.7), it follows that

$$\frac{1}{\sqrt{\pi t}} + \operatorname{erfc}\left(\frac{1}{\sqrt{t}}\right) < \kappa_1 < \frac{1}{\sqrt{\pi t}} + 1.$$

As $t \to 0$,

$$\operatorname{erfc}\left(\frac{1}{\sqrt{t}}\right) = \frac{\sqrt{t}}{\sqrt{\pi}} e^{-1/t}\left(1 - \frac{t}{2} + \cdots\right)$$

is exponentially small, and so

$$\kappa_1 \sim \frac{1}{\sqrt{\pi t}} \quad \text{as} \quad t \to 0. \tag{5.1}$$

Now considering κ_2, using lower Riemann sums as illustrated in Fig. 5.2(a) gives

$$2\sum_{n=1}^{\infty} e^{-(2n-1)^2/4t} > \int_1^{\infty} e^{-x^2/4t}\, dx = \sqrt{\pi t}\operatorname{erfc}\left(\frac{1}{2\sqrt{t}}\right),$$

so from (3.8) it follows that

$$\kappa_2 > \frac{1}{2}\operatorname{erfc}\left(\frac{1}{2\sqrt{t}}\right).$$

Similarly, using upper Riemann sums, Fig. 5.2(b) shows that

$$2\sum_{n=2}^{\infty} e^{-(2n-1)^2/4t} < \int_1^{\infty} e^{-x^2/4t}\, dx = \sqrt{\pi t}\operatorname{erfc}\left(\frac{1}{2\sqrt{t}}\right).$$

Note that we may re-write (3.8) in the form

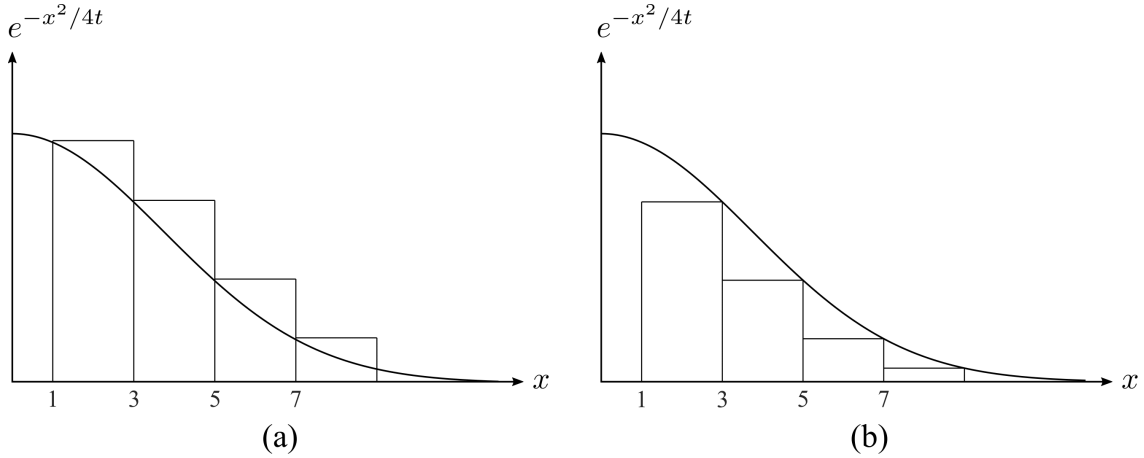

Figure 5.2: Schematic drawing illustrating the area under the curve $e^{-x^2/4t}$ and an approximation to this area using lower (a) and upper (b) Riemann sums.

$$\kappa_2 = \frac{1}{\sqrt{\pi t}}\left(e^{-1/4t} + \sum_{n=2}^{\infty} e^{-(2n-1)^2/4t}\right),$$

so it follows that

$$\kappa_2 < \frac{1}{\sqrt{\pi t}} e^{-1/4t} + \frac{1}{2}\operatorname{erfc}\left(\frac{1}{2\sqrt{t}}\right).$$

Thus, we have

$$\frac{1}{2}\operatorname{erfc}\left(\frac{1}{2\sqrt{t}}\right) < \kappa_2 < \frac{1}{\sqrt{\pi t}} e^{-1/4t} + \frac{1}{2}\operatorname{erfc}\left(\frac{1}{2\sqrt{t}}\right).$$

As $t \to 0$,

$$\operatorname{erfc}\left(\frac{1}{2\sqrt{t}}\right) = \frac{2\sqrt{t}}{\sqrt{\pi}} e^{-1/4t}\left(1 - 2t + \cdots\right)$$

is exponentially small, and $e^{-1/4t}$ decays faster than $1/\sqrt{\pi t}$ grows. Therefore, as $t \to 0$, κ_2 is exponentially small and the coupled Volterra integral equations (3.9) and (3.10) become

$$\begin{aligned} c(0,t) &\sim 1 + \mu \int_0^t \kappa_1(t-\tau)\big[1 - c(0,\tau)\big]\, d\tau, \\ c(1,t) &\sim 1 - \alpha \int_0^t \kappa_1(t-\tau)\frac{c(1,\tau)}{1+\beta c(1,\tau)}\, d\tau. \end{aligned} \tag{5.2}$$

Using result (5) in [14], it may be shown that

$$\frac{1}{\sqrt{\pi t}}\left(1 + 2\sum_{n=1}^{\infty} e^{-n^2/t}\right) = 1 + 2\sum_{n=1}^{\infty} e^{-n^2\pi^2 t},$$

or $\kappa_1 = k_0(1,t)$. Thus, for small t, (5.2) is equivalent to (3.6), the Volterra integral equation derived for the special case when $\mu = 0$. This means the small t approximate solution that we are about to derive will be independent of μ. This makes sense: in order for mass transfer to take place across the fluid/air interface (i.e. for the flux to be non-zero), a gradient of solute must first be generated via diffusion and metabolism. However, for very early times, no such gradient will yet exist and this is equivalent to setting $\mu = 0$.

Now, for $t \to 0$, we consider the following expansion:

$$c(1,t) = a_1 + a_2 t^{1/2} + a_3 t + a_4 t^{3/2} + \mathcal{O}(t^2). \tag{5.3}$$

Substituting (5.3) into (5.2) and making use of (5.1) yields

$$
\begin{aligned}
&a_1 + a_2 t^{1/2} + a_3 t + a_4 t^{3/2} + \mathcal{O}(t^2) \\
&= 1 - \frac{\alpha}{\sqrt{\pi}} \int_0^t (t-\tau)^{-1/2} \big[a_1 + a_2 \tau^{1/2} + a_3 \tau + a_4 \tau^{3/2} + \mathcal{O}(t^2) \big] \\
&\quad \times \left[\frac{1}{a_1\beta + 1} - \frac{a_2 \beta}{(a_1\beta+1)^2} \tau^{1/2} + \frac{(a_2^2 - a_1 a_3)\beta^2 - a_3 \beta}{(a_1\beta+1)^3} \tau + \mathcal{O}(\tau^{3/2}) \right] \, d\tau.
\end{aligned}
$$

Multiplying out the brackets, collecting terms and integrating, then finally equating powers of t gives

$$
\begin{aligned}
a_1 &= 1, \\
a_2 &= -\frac{2\alpha}{\sqrt{\pi}(\beta+1)}, \\
a_3 &= \frac{\alpha^2}{(\beta+1)^3}, \\
a_4 &= -\frac{4\alpha^3(\pi - 4\beta)}{3\pi^{3/2}(\beta+1)^5}.
\end{aligned}
$$

Thus, from (5.3), the approximate solution for $t \to 0$ is given by

$$
c(1,t) = 1 - \frac{2\alpha}{\sqrt{\pi}(\beta+1)} t^{1/2} + \frac{\alpha^2}{(\beta+1)^3} t - \frac{4\alpha^3(\pi - 4\beta)}{3\pi^{3/2}(\beta+1)^5} t^{3/2} + \mathcal{O}(t^2). \tag{5.4}
$$

5.2 Steady-state solution

As $t \to \infty$, the solution of the diffusion equation subject to (2.7) and (2.8) is given by

$$
c(x, \infty) = A - \mu(1 - A)x, \tag{5.5}
$$

where A is the positive root of the following quadratic equation:

$$
\mu\beta(\mu+1)A^2 + \big[\mu(1 - \beta(1+2\mu)) + \alpha(\mu+1)\big]A + \mu(\mu\beta - \alpha - 1) = 0. \tag{5.6}
$$

Note that for the special case when $\mu = 0$, (5.6) reduces to $A = 0$ and thus the steady-state solution is equal to zero; this is intuitive, since without replenishment the solute will fully deplete due to metabolism by the cells.

6 Results and discussion

In this section, we compare the numerical solution of the Volterra integral equation (3.5), or (3.6) for the special case when $\mu = 0$, with the small β, large β, small t and steady-state solutions. It is noted

that our approach of obtaining solutions by solving the integral equations numerically provides the solutions directly at the cell surface. Moreover, since (3.5) and (3.6) are *convolution* Volterra integral equations, solving these via product integration methods is more computationally efficient (both in terms of storage as well as operation count) than using standard numerical techniques to solve the original PDE system (see, e.g. [15]). For details of the numerical methods employed to obtain the solutions of the Volterra integral equations (including those that appear in the $c_1(1,t)$ term of the small β solutions), the reader is referred to the supplementary information.

We begin by exploring numerically the influence of μ on the cell surface solute concentration given by (3.5), or (3.6) for the special case when $\mu = 0$, assuming baseline values of $\alpha = \beta = 1$. In Fig. 6.1, we observe the independence of the cell surface solute concentration on μ at early times, in agreement with (5.4). Moreover, as expected, increasing the value of μ results in higher cell surface solute concentrations at later times. It is notable that, in line with (5.5), $c(1,t)$ appears to be tending towards a non-zero steady-state value as $\mu \to \infty$, and towards zero as $\mu \to 0$; computations performed over a larger time interval confirm that the steady-state solutions are reached.

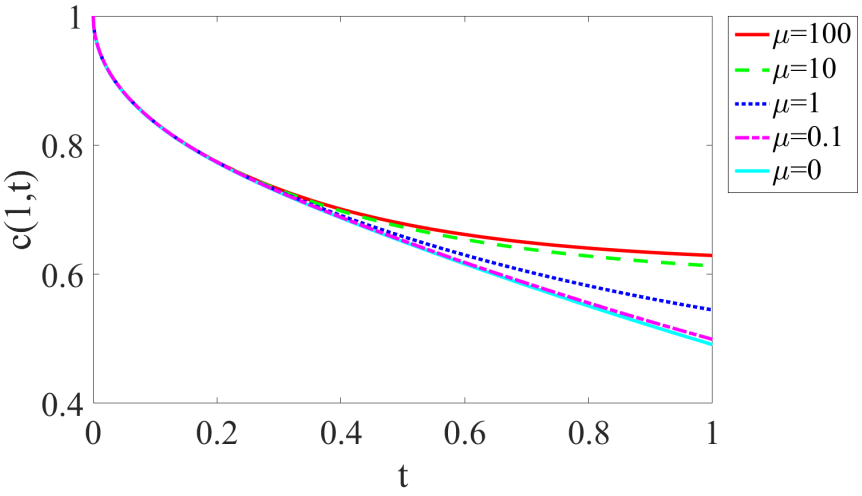

Figure 6.1: Numerical solution of the Volterra integral equation (3.5) with $\mu = 0.1 - 100$, and numerical solution of the Volterra integral equation (3.6) for the case when $\mu = 0$, for $0 \leq t \leq 1$ with $\alpha = \beta = 1$.

Next, we explore numerically the effect of α on the cell surface solute concentration given by (3.5), assuming baseline values of $\mu = \beta = 1$. Since α is the ratio of the metabolic rate and the diffusion rate, it is expected that as α increases, and therefore as the metabolic rate increases, the rate of solute depletion will increase. This behaviour is observed in Fig. 6.2, where it is clear that for the smallest value of α, i.e. for negligible metabolism, the solute concentration remains high, whereas for the largest value of α, i.e. for high metabolism, the solute concentration rapidly decreases. It is noted that Fig. 6.2 can also be used to anticipate changes to the solute concentration in the event of a cell population increase: since the cell density is incorporated within V_{max}, an

increase in cell population and therefore cell density will lead to an increased metabolic rate, i.e. an increased value of α.

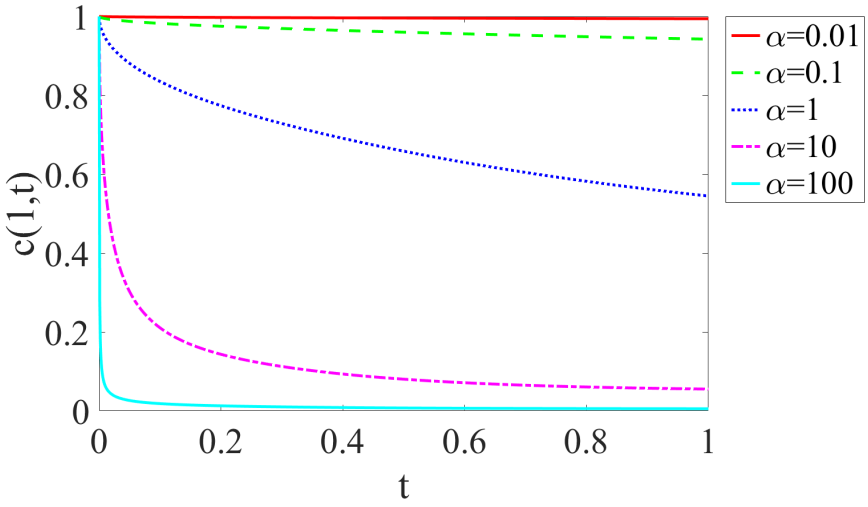

Figure 6.2: Numerical solution of the Volterra integral equation (3.5) with $\alpha = 0.01 - 100$, for $0 \leq t \leq 1$ with $\mu = \beta = 1$.

Now, for both extremes of μ, we compare the small β solutions with the numerical solutions to the Volterra integral equations, for a baseline value of $\alpha = 1$. For the case when $\mu = 0$, the numerical solution of (3.6) is compared with the small β solution (4.7) (Fig. 6.3, left), and for the case when $\mu \to \infty$, the numerical solution of (3.5) is compared with the small β solution (4.6) (Fig. 6.3, right). Note that, in practice, $\mu = 10^6$ was used to generate plots for the case when $\mu \to \infty$. In Fig. 6.3, we observe that as β is reduced from 1 to 0.01, the agreement between the numerical solutions and the approximate small β solutions improves. It is noted that, whilst there is a large discrepancy between the numerical solutions and the small β solutions up to $\mathcal{O}(1)$ for $\beta = 1$, the approximate solutions up to $\mathcal{O}(\beta)$ are good, with only a small discrepancy evident at early times. For $\beta = 0.1$, the $\mathcal{O}(\beta)$ solutions are in excellent agreement with the numerical solutions, whilst for $\beta = 0.01$, the $\mathcal{O}(1)$ solutions are sufficient.

Similarly, for a baseline value of $\alpha = 1$, we compare the numerical solutions of (3.6) and (3.5) with the large β solutions (4.11) and (4.10), for the case when $\mu = 0$ (Fig. 6.4, left) and $\mu \to \infty$ (Fig. 6.4, right) , respectively. Note that, in practice, $\mu = 10^6$ was used to generate plots for the case when $\mu \to \infty$. In Fig. 6.4, the large β approximate solutions vary substantially from the numerical solutions to the Volterra integral equations when $\beta = 1$. However, we observe that as β is increased to 10, and subsequently 100, the agreement between the approximate solutions and the numerical solutions notably improves. For $\beta = 10$, whilst there is a small discrepancy between the numerical solutions and the large β solutions up to $\mathcal{O}(1/\beta)$, the approximate solutions up to $\mathcal{O}(1/\beta^2)$ are excellent. For $\beta = 100$, the $\mathcal{O}(1/\beta)$ solutions are sufficient.

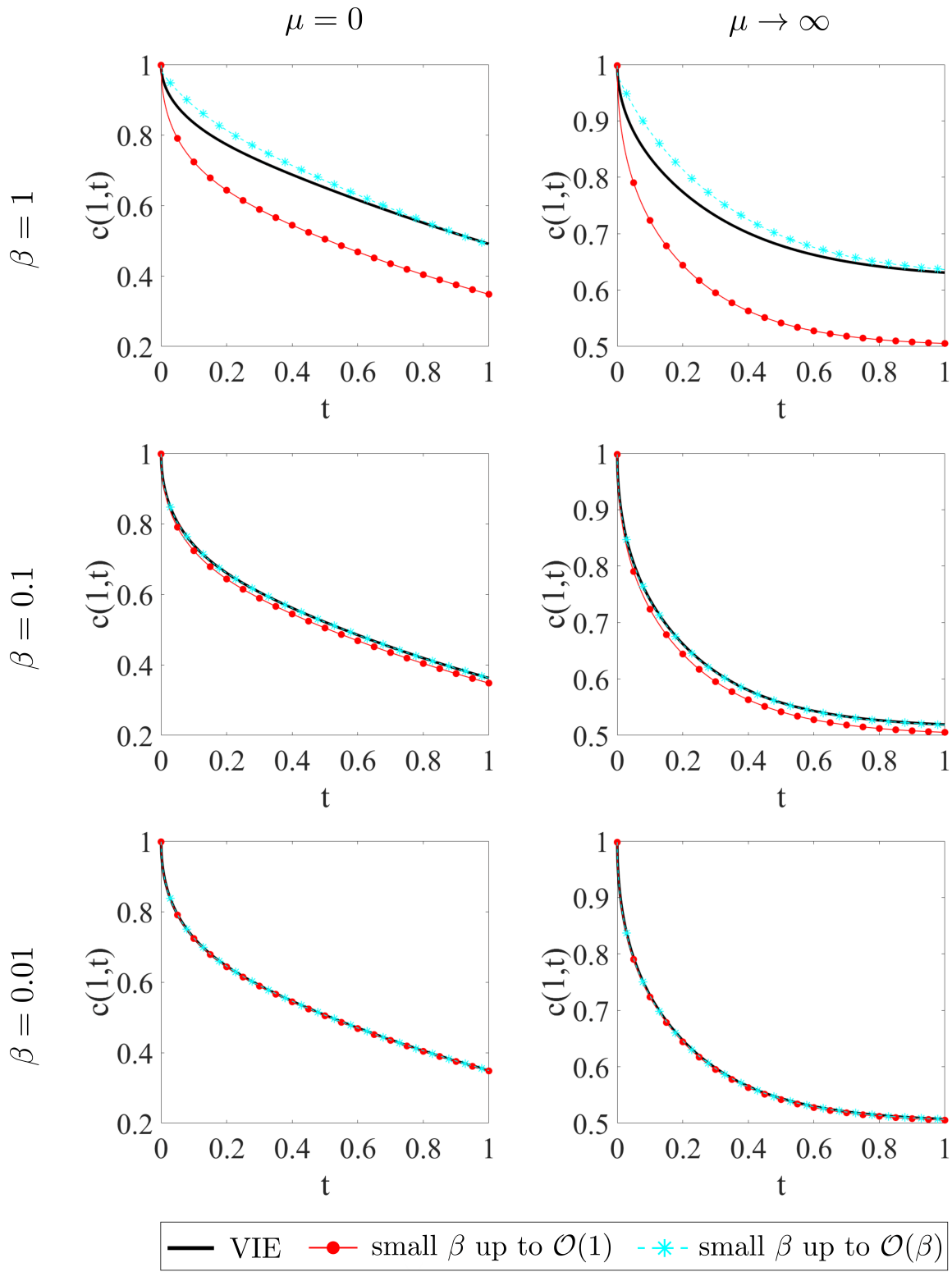

Figure 6.3: Comparison between the numerical solution of the Volterra integral equation (3.6) and the small β approximate solution (4.7) for the case when $\mu = 0$ (left), and comparison between the numerical solution of the Volterra integral equation (3.5) and the small β approximate solution (4.6) for $\mu \to \infty$ (right), for $0 \leq t \leq 1$ with $\alpha = 1$, and $\beta = 1$ (upper), $\beta = 0.1$ (middle) and $\beta = 0.01$ (lower). Note that, in practice, $\mu = 10^6$ was used to generate plots for the case when $\mu \to \infty$.

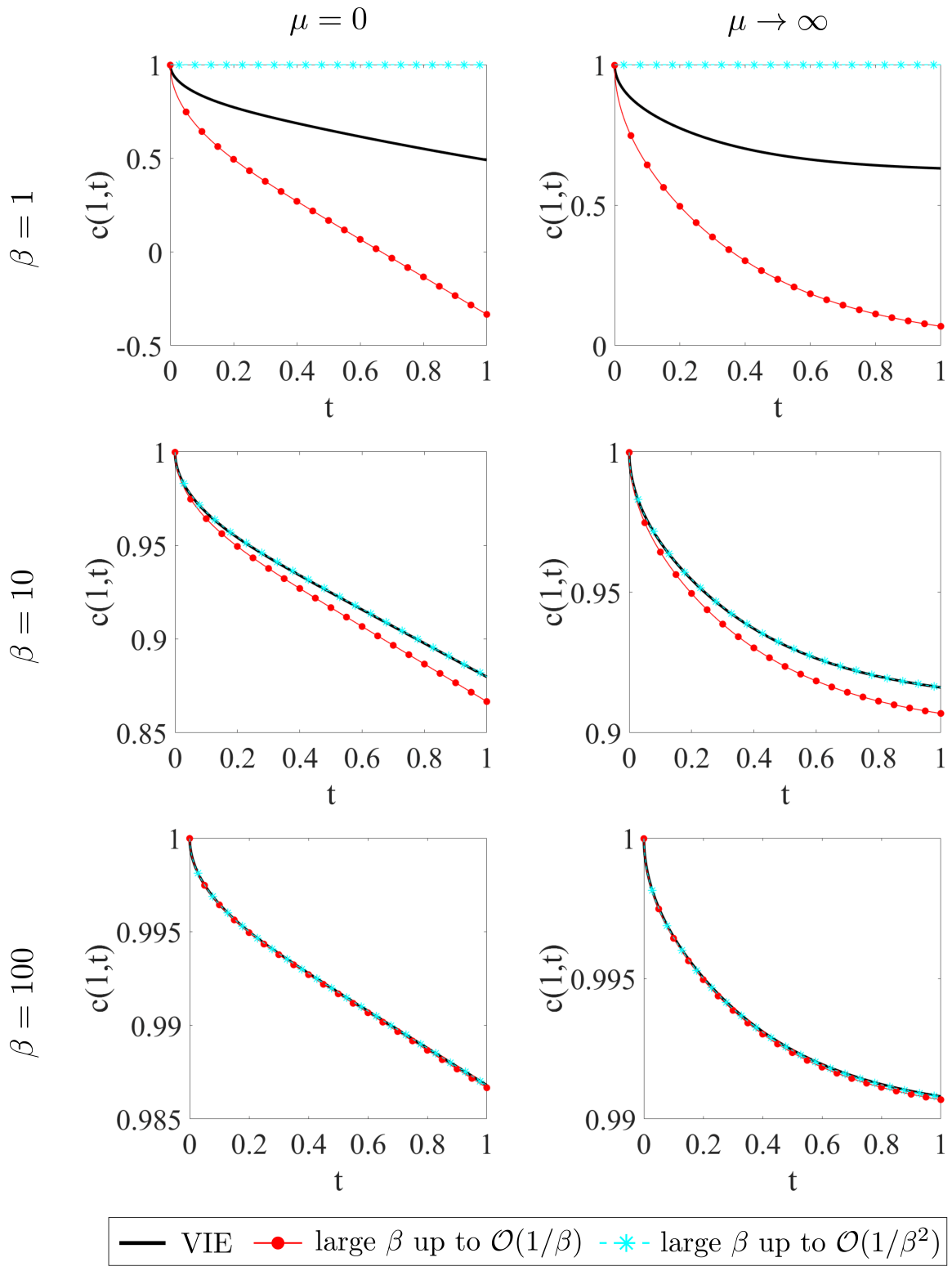

Figure 6.4: Comparison between the numerical solution of the Volterra integral equation (3.6) and the large β approximate solution (4.11) for the case when $\mu = 0$ (left), and comparison between the numerical solution of the Volterra integral equation (3.5) and the large β approximate solution (4.10) for $\mu \to \infty$ (right), for $0 \leq t \leq 1$ with $\alpha = 1$, and $\beta = 1$ (upper), $\beta = 10$ (middle) and $\beta = 100$ (lower). Note that, in practice, $\mu = 10^6$ was used to generate plots for the case when $\mu \to \infty$.

Now, using baseline values of $\alpha = \beta = \mu = 1$, Fig. 6.5 compares the numerical solution of the Volterra integral equation (3.5) with the small t solution (5.4). As expected, as we increase the number of terms in the approximate solution, we observe better agreement with the numerical solution. While there is a small discrepancy between the numerical solution and the small t solution up to $\mathcal{O}(t^{1/2})$, the inclusion of the $\mathcal{O}(t)$ term results in excellent agreement.

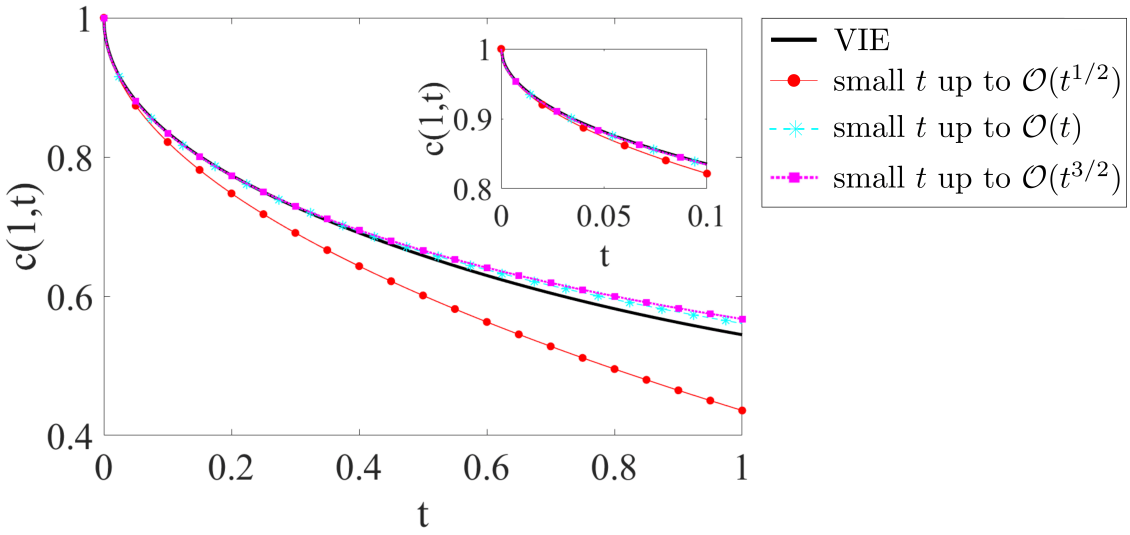

Figure 6.5: Comparison between the numerical solution of the Volterra integral equation (3.5) and the small t approximate solution (5.4), for $0 \leq t \leq 1$ with $\alpha = \beta = \mu = 1$. The inset plot highlights the excellent agreement between the solutions for $0 \leq t \leq 0.1$.

Finally, we use realistic parameter values from the literature (listed in Table 2.2) to compare the numerical solutions of the Volterra integral equations with the approximate solutions and steady-state solutions. For the parameter values relating to O_2 metabolism (case 1), Fig. 6.6 shows excellent agreement when comparing the numerical solution of the Volterra integral equation (3.5) with the large β approximate solution (4.10) and the non-zero steady-state solution (5.5). For the parameter values relating to drug metabolism (case 2), Fig. 6.7 compares the numerical solution of the Volterra integral equation (3.6) with the small β approximate solution (4.7) and the steady-state solution of zero. For this case, some discrepancy is noted between the numerical solution and the small β solution up to $\mathcal{O}(1)$, but the small β solution up to $\mathcal{O}(\beta)$ provides excellent agreement. In both cases, the steady-state solutions are obtained.

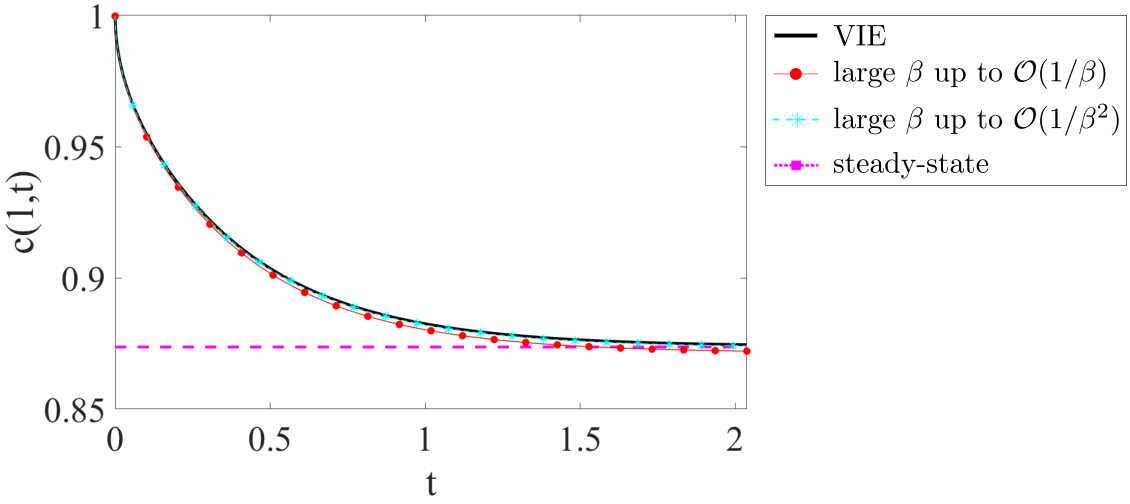

Figure 6.6: Comparison between the numerical solution of the Volterra integral equation (3.5), the steady-state solution (5.5) and the large β approximate solution (4.10), using the parameter values from Table 2.2 that correspond to O_2. Note that $\mu = 10^6$ was chosen to represent a constant supply of O_2 from the air, and the maximum non-dimensional time corresponds to 6 hours.

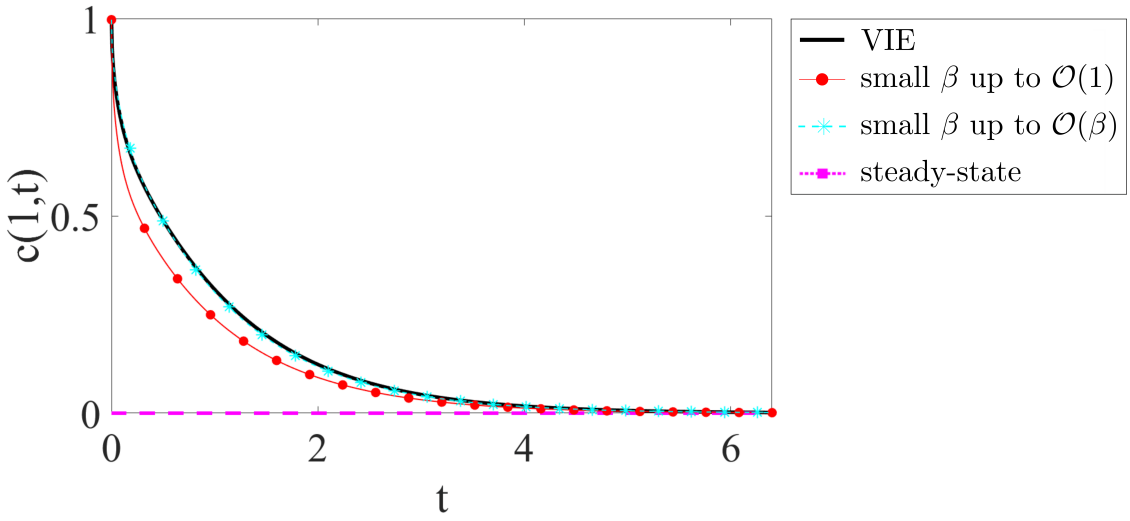

Figure 6.7: Comparison between the numerical solution of the Volterra integral equation (3.6), the steady-state solution (i.e. zero) and the small β approximate solution (4.7) using the parameter values from Table 2.2 that correspond to drugs primarily metabolised in the liver. Note that $\mu = 0$ was chosen to represent no supply of drug from the air, and the maximum non-dimensional time corresponds to 2 days.

7 Utility of the model

In this paper, Volterra integral equations were derived for estimating the solute concentration at the surface of a layer of cells cultured within a petri dish. Whilst solutions can be obtained by solving

(3.5) and (3.6) directly using numerical schemes (see supplementary information), this does not provide a detailed insight into the dependency of the solution on key model parameters; instead, this information was gained by applying analytical methods to derive approximate solutions, valid for small β, large β and small t, as well as the steady-state solution. The analytical solutions can be used to quickly obtain details of the cell culture environment that could not be uncovered by numerical solutions alone, without requiring the implementation of complicated numerical techniques.

To expand upon the utility of the results presented here, further simple relationships are provided for answering key questions that could lead to the improvement of *in vitro* cell culture conditions. This would be of particular relevance to experimental researchers who wish to reap the benefits of modelling without requiring a deep understanding of the underlying mathematical techniques.

Question 1: How much solute has been metabolised at each stage of the experiment?

In dimensional parameters, the total amount of solute that has been metabolised in a given time may be calculated by integrating the M-M reaction term as follows:

$$m(T) = A \int_0^T \frac{V_{max} c(d,t)}{K_m + c(d,t)}\, dt,$$

where $m(T)$ (mol) is the total amount of solute that has been metabolised in a given time, T (s) is the time of interest, and A (m^2) is the area covered by the cells. In order to make use of the solutions presented in this chapter, we non-dimensionalise this expression using the scalings

$$c = c_0 c', \quad t = \frac{d^2}{D} t',$$

to obtain

$$m(T) = \int_0^T \frac{\alpha c(1,t)}{1 + \beta c(1,t)}\, dt,$$

where the primes have been dropped for convenience. In general, $m(T)$ may be calculated by solving (3.5) numerically to obtain $c(1,t)$, and then performing the integration. However, it is noted that when β is either small or large, M-M reduces to linear kinetics and so

$$m(T) \sim \begin{cases} \displaystyle\int_0^T \alpha c(1,t)\, dt, & \beta \to 0 \\ \displaystyle\int_0^T \frac{\alpha}{\beta}\, dt, & \beta \to \infty \end{cases}.$$

For the case when $\beta \to 0$, we can approximate $m(T)$ by replacing $c(1,t)$ by the small β solution

(4.6) before performing the integration to obtain

$$m(T) \sim \alpha \left(\frac{\mu T}{\alpha\mu + \alpha + \mu} + \sum_{n=1}^{\infty} \frac{2\big[\mu\cos(\lambda_n) - \lambda_n \sin(\lambda_n)\big]\big[1 - e^{-\lambda_n^2 T}\big]}{\lambda_n^2\big[(\alpha\mu + \alpha + \mu - \lambda_n^2)\cos(\lambda_n) - \lambda_n(2 + \alpha + \mu)\sin(\lambda_n)\big]} + \mathcal{O}(\beta) \right). \tag{7.1}$$

For the special case when $\mu = 0$, $c(1,t)$ can be replaced by (4.7) and the integration can be performed to give

$$m(T) \sim \alpha \left(\sum_{n=1}^{\infty} \frac{2\sin(\chi_n)\big[1 - e^{-\chi_n^2 T}\big]}{\chi_n^2\left[\chi_n\cos(\chi_n) + (\chi + 1)\sin(\chi_n)\right]} + \mathcal{O}(\beta) \right). \tag{7.2}$$

For the case when $\beta \to \infty$, solute metabolism is approximately constant and so $m(T)$ is simply approximated by

$$m(T) \sim \frac{\alpha}{\beta} T. \tag{7.3}$$

Thus, the non-dimensional amount of solute that has been metabolised in a given time may be approximated by

- (7.1) when β is small, for a general value of μ, or
- (7.2) when β is small, for the special case when $\mu = 0$, or
- (7.3) when β is large.

The dimensional amount of solute that has been metabolised in a given time can then easily be obtained by multiplying $m(T)$ by Adc_0, recalling that d (m) is the depth of the fluid and c_0 (mol m^{-3}) is the initial solute concentration.

Question 2: How can the experiment be configured so that the cell surface solute concentration remains above a desired concentration for a given time?

To ensure that the solute concentration at the cell surface remains above a desired amount for a specified duration of time, the underlying model parameters must be configured such that the following inequality is satisfied:

$$c(1,T) > c_D, \tag{7.4}$$

where c_D is the non-dimensional desired cell surface solute concentration. When β is either small or large, we can replace $c(1,T)$ by the approximate analytical solutions derived in sections 4.1 and 4.2, and the values of α, β and/or μ should be adjusted such that (7.4) is satisfied. In practice, this

means altering the depth of the fluid and/or the initial solute concentration, since the remaining dimensional parameters that α, β and μ are comprised of relate specifically to the cell type and solute under consideration.

Question 3: How long does it take for the cell surface solute concentration to reach steady-state?

The non-dimensional time taken for the solute concentration at the cell surface to reach a desired amount may be obtained by solving

$$c(1,t) = c_D. \tag{7.5}$$

In general, we can solve this equation by using the numerical solution of the Volterra integral equation, but again, when β is either small or large, we can instead replace $c(1,t)$ by the approximate analytical solutions. Thus, the non-dimensional time taken to reach a desired cell surface solute concentration may be approximated by solving (7.5) for t, with $c(1,t)$ replaced by

- (4.6) when β is small, for a general value of μ, or
- (4.7) when β is small, for the special case when $\mu = 0$, or
- (4.10) when β is large, for a general value of μ, or
- (4.11) when β is large, for the special case when $\mu = 0$.

The time in seconds can then easily be obtained by simply multiplying t by d^2/D, recalling that D ($\mathrm{m}^2\ \mathrm{s}^{-1}$) is the diffusion coefficient of the solute.

To calculate how long it takes for the solute concentration at the cell surface to reach steady-state, the above steps may be followed with c_D replaced by the cell surface solute concentration as $t \to \infty$, given by (5.5). Recall that for the special case when $\mu = 0$, the steady-state cell surface solute concentration is equal to zero, and so the non-dimensional time taken to reach steady-state may be calculated by solving $c(1,t) = 0$, or equivalently, $m(t) = 1$, since the solute will be fully depleted when the amount of solute metabolised is equal to the initial amount of solute.

References

[1] K. Duval, H. Grover, L.-H. Han, Y. Mou, A. F. Pegoraro, J. Fredberg, and Z. Chen. Modeling Physiological Events in 2D vs. 3D Cell Culture. *Physiology*, 32:266–277, 2017. doi: 10.1152/physiol.00036.2016.

[2] R. Edmondson, J. J. Broglie, A. F. Adcock, and L. Yang. Three-Dimensional Cell Culture Systems and Their Applications in Drug Discovery and Cell-Based Biosensors. *ASSAY Drug Dev Technol*, 12(4):207–218, 2014. doi: 10.1089/adt.2014.573.

[3] J. F. Wong, C. A. Simmons, and E. W. K. Young. Modeling and Measurement of Biomolecular Transport and Sensing in Microfluidic Cell Culture and Analysis Systems. In *Modeling of Microscale Transport in Biological Processes*. Academic Press, 2017. ISBN 978-0-12-804595-4.

[4] E. L. LeCluyse, R. P. Witek, M. E. Andersen, and M. J. Powers. Organotypic liver culture models: meeting current challenges in toxicity testing. *Crit Rev Toxicol*, 42(6):501–548, 2012. doi: 10.3109/10408444.2012.682115.

[5] J. Demol, D. Lambrechts, L. Geris, J. Schrooten, and H. Van Oosterwyck. Towards a quantitative understanding of oxygen tension and cell density evolution in fibrin hydrogels. *Biomaterials*, 32:107–118, 2011. doi: 10.1016/j.biomaterials.2010.08.093.

[6] F. Zhao, P. Pathi, W. Grayson, Q. Xing, B. R. Locke, and T. Ma. Effects of Oxygen Transport on 3-D Human Mesenchymal Stem Cell Metabolic Activity in Perfusion and Static Cultures: Experiments and Mathematical Model. *Biotechnol Prog*, 21:1269–1280, 2005. doi: 10.1021/bp0500664.

[7] A. Przekwas and M. R. Somayaji. Computational pharmacokinetic modeling of organ-on-chip devices and microphysiological systems. In *Organ-on-a-chip*. Academic Press, 2020. ISBN 978-0-12-817202-5.

[8] I. Burova, C. Peticone, D. De Silva Thompson, J. C. Knowles, I. Wall, and R. J. Shipley. A parameterised mathematical model to elucidate osteoblast cell growth in a phosphate-glass microcarrier culture. *J Tissue Eng*, 10:2041731419830264, 2019. doi: 10.1177/2041731419830264.

[9] M. L. Yarmush, M. Toner, J. C. Y. Dunn, A. Rotem, A. Hubel, and R. G. Tompkins. Hepatic Tissue Engineering: Development of Critical Technologies. *Ann N Y Acad Sci*, 665:238–252, 1992. doi: 10.1111/j.1749-6632.1992.tb42588.x.

[10] J. R. Cannon. *The One-Dimensional Heat Equation*. Cambridge University Press, Cambridge, UK, 1984. ISBN 978-0-521-30243-2.

[11] https://www.corning.com/catalog/cls/documents/application-notes/CLS-AN-209.pdf. Accessed: Jun-2022.

[12] J. A. Leedale, J. A. Kyffin, A. L. Harding, H. E. Colley, C. Murdoch, P. Sharma, D. P. Williams, S. D. Webb, and R. N. Bearon. Multiscale modelling of drug transport and metabolism in liver spheroids. *Interface Focus*, 10:20190041, 2019. doi: 10.1098/rsfs.2019.0041.

[13] R. Milo and R. Phillips. *Cell Biology by the Numbers*. Garland Science, New York, NY, 2015. ISBN 978-0-8153-4537-4.

[14] B. Jumarhon, S. McKee, and T. Tang. The proof of an inequality arising in a reaction-diffusion study in a small cell. *J Comp App Math*, 51:99–101, 1994. doi: 10.1016/0377-0427(94)90092-2.

[15] H. Brunner. *Volterra Integral Equations: An Introduction to Theory and Applications*. Cambridge University Press, Cambridge, UK, 2017. ISBN 978-1-316-16249-1.

Supplementary information for "Solute transport with Michaelis-Menten kinetics for *in vitro* cell culture"

Lauren Hyndman[1], Sean McKee[2], and Sean McGinty[1*]

[1]Division of Biomedical Engineering, University of Glasgow, Glasgow G12 8QQ, UK.

[2]Department of Mathematics and Statistics, University of Strathclyde, Glasgow G1 1XQ, UK.

[*]Corresponding author. Tel.: +44 141 3308588. Email address: sean.mcginty@glasgow.ac.uk.

Solutions to the linear PDE models

For $\beta \ll 1$ and $\beta \gg 1$, the nonlinear M-M kinetics may be linearised and the following PDE models can be solved directly to obtain approximate solutions that are valid for small and large β:

$$\frac{\partial c}{\partial t}(x,t) = \frac{\partial^2 c}{\partial x^2}(x,t), \quad 0 < x < 1, \quad t > 0, \tag{1}$$

$$c(x,0) = 1, \quad 0 < x < 1, \tag{2}$$

$$\frac{\partial c}{\partial x}(0,t) = -\mu\big[1 - c(0,t)\big], \quad t > 0, \tag{3}$$

$$\frac{\partial c}{\partial x}(1,t) = \begin{cases} -\alpha c(1,t), & \beta \ll 1, \quad (4) \\ -\dfrac{\alpha}{\beta}, & \beta \gg 1. \quad (5) \end{cases}$$

Solving (1) subject to (2) and (3) gives

$$\bar{c}(x,s) = a(s)\cosh(\sqrt{s}x) + \frac{\mu a(s)}{\sqrt{s}}\sinh(\sqrt{s}x) + \frac{1}{s}. \tag{6}$$

and taking the inverse Laplace transform yields

$$c(x,t) = 1 + \mathcal{L}^{-1}\left\{a(s)\left[\cosh(\sqrt{s}x) + \frac{\mu}{\sqrt{s}}\sinh(\sqrt{s}x)\right]\right\}. \tag{7}$$

We may now apply (4) and (5) in turn to obtain small and large β solutions.

Small β solution. Here, we obtain $a(s)$ by differentiating (6) with respect to x and applying the Laplace transform of (4):

$$a(s) = -\frac{\alpha}{\sqrt{s}\big[(s+\alpha\mu)\sinh(\sqrt{s}) + \sqrt{s}(\alpha+\mu)\cosh(\sqrt{s})\big]}.$$

Then, from (7), it follows that

$$c(x,t) = 1 - \alpha\mathcal{L}^{-1}\left\{\frac{\sqrt{s}\cosh(\sqrt{s}x) + \mu\sinh(\sqrt{s}x)}{s\big[(s+\alpha\mu)\sinh(\sqrt{s}) + \sqrt{s}(\alpha+\mu)\cosh(\sqrt{s})\big]}\right\}. \tag{8}$$

It may readily be shown that no branch points exist, so the residue theorem is used to evaluate the inverse Laplace transform. The poles are given by

$$s = 0 \quad \text{and} \quad (s+\alpha\mu)\sinh(\sqrt{s}) + \sqrt{s}(\alpha+\mu)\cosh(\sqrt{s}) = 0,$$

and, for convenience, setting $\sqrt{s} = i\lambda$ in the transcendental equation gives

$$(\alpha\mu - \lambda^2)\sin(\lambda) + \lambda(\alpha+\mu)\cos(\lambda) = 0. \tag{9}$$

Hence, there is a simple pole at $s = 0$ and infinitely many simple poles at $s_n = -\lambda_n^2$ for $n \in \mathbb{N}$, where λ_n are the roots of (9). Using L'Hôpital's rule to calculate the residues gives

$$\operatorname*{Res}_{s=0} = \frac{\mu x + 1}{\alpha\mu + \alpha + \mu},$$
$$\operatorname*{Res}_{s=s_n} = \frac{2\big[\lambda_n\cos(\lambda_n x) + \mu\sin(\lambda_n x)\big]}{\lambda_n\big[(\alpha\mu+\alpha+\mu-\lambda_n^2)\cos(\lambda_n) - \lambda_n(2+\alpha+\mu)\sin(\lambda_n)\big]}e^{-\lambda_n^2 t}.$$

Then, by applying the residue theorem, it follows from (8) that

$$c(x,t) = 1 - \alpha\left(\frac{\mu x+1}{\alpha\mu+\alpha+\mu} + \sum_{n=1}^{\infty}\frac{2\big[\lambda_n\cos(\lambda_n x) + \mu\sin(\lambda_n x)\big]}{\lambda_n\big[(\alpha\mu+\alpha+\mu-\lambda_n^2)\cos(\lambda_n) - \lambda_n(2+\alpha+\mu)\sin(\lambda_n)\big]}e^{-\lambda_n^2 t}\right).$$

Re-arranging (9) to obtain

$$-\alpha\big[\lambda_n\cos(\lambda_n) + \mu\sin(\lambda_n)\big] = \lambda_n\big[\mu\cos(\lambda_n) - \lambda_n\sin(\lambda_n)\big],$$

and choosing $x = 1$ results in

$$c(1,t) = \frac{\mu}{\alpha\mu+\alpha+\mu} + \sum_{n=1}^{\infty}\frac{2\big[\mu\cos(\lambda_n) - \lambda_n\sin(\lambda_n)\big]}{(\alpha\mu+\alpha+\mu-\lambda_n^2)\cos(\lambda_n) - \lambda_n(2+\alpha+\mu)\sin(\lambda_n)}e^{-\lambda_n^2 t},$$

i.e. the small β solution (4.6), to leading-order.

Large β solution. Here, we obtain $a(s)$ by differentiating (6) with respect to x and applying the Laplace transform of (5):

$$a(s) = -\frac{\alpha}{\beta s\big[\sqrt{s}\sinh(\sqrt{s}) + \mu\cosh(\sqrt{s})\big]}.$$

Then, from (7), it follows that

$$c(x,t) = 1 - \frac{\alpha}{\beta}\mathcal{L}^{-1}\left\{\frac{\sqrt{s}\cosh(\sqrt{s}x) + \mu\sinh(\sqrt{s}x)}{s^{3/2}\big[\sqrt{s}\sinh(\sqrt{s}) + \mu\cosh(\sqrt{s})\big]}\right\}. \tag{10}$$

It may readily be shown that no branch points exist, so the residue theorem is used to evaluate the inverse Laplace transform. The poles are given by

$$s = 0 \quad \text{and} \quad \sqrt{s}\sinh(\sqrt{s}) + \mu\cosh(\sqrt{s}) = 0,$$

and, for convenience, setting $\sqrt{s} = i\gamma$ in the transcendental equation gives

$$\mu\cos(\gamma) - \gamma\sin(\gamma) = 0. \tag{11}$$

Hence, there is a simple pole at $s = 0$ and infinitely many simple poles at $s_n = -\gamma_n^2$ for $n \in \mathbb{N}$, where γ_n are the roots of (11). Using L'Hôpital's rule to calculate the residues gives

$$\operatorname*{Res}_{s=0} = x + \frac{1}{\mu},$$
$$\operatorname*{Res}_{s=s_n} = -\frac{2\big[\gamma_n\cos(\gamma_n x) + \mu\sin(\gamma_n x)\big]}{\gamma_n^2\big[\gamma_n\cos(\gamma_n) + (\mu+1)\sin(\gamma_n)\big]}e^{-\gamma_n^2 t}.$$

Then, by applying the residue theorem, it follows from (10) that

$$c(x,t) = 1 - \frac{\alpha}{\beta}\left(x + \frac{1}{\mu} - \sum_{n=1}^{\infty}\frac{2\big[\gamma_n\cos(\gamma_n x) + \mu\sin(\gamma_n x)\big]}{\gamma_n^2\big[\gamma_n\cos(\gamma_n) + (\mu+1)\sin(\gamma_n)\big]}e^{-\gamma_n^2 t}\right).$$

Choosing $x = 1$ results in

$$c(1,t) = 1 - \frac{\alpha}{\beta}\left(1 + \frac{1}{\mu} - \sum_{n=1}^{\infty}\frac{2\big[\gamma_n\cos(\gamma_n) + \mu\sin(\gamma_n)\big]}{\gamma_n^2\big[\gamma_n\cos(\gamma_n) + (\mu+1)\sin(\gamma_n)\big]}e^{-\gamma_n^2 t}\right),$$

which may be shown to be equivalent to the large β solution (4.10), to first-order.

Solutions to the linear PDE models for the case when $\mu = 0$

For the special case when $\mu = 0$, we have a zero flux boundary condition at the fluid/air interface. Thus, the following PDE models can be solved directly to obtain approximate solutions that are valid for $\beta \ll 1$ and $\beta \gg 1$:

$$\frac{\partial c}{\partial t}(x,t) = \frac{\partial^2 c}{\partial x^2}(x,t), \quad 0 < x < 1, \quad t > 0, \tag{12}$$

$$c(x,0) = 1, \quad 0 < x < 1, \tag{13}$$

$$\frac{\partial c}{\partial x}(0,t) = 0, \quad t > 0, \tag{14}$$

$$\frac{\partial c}{\partial x}(1,t) = \begin{cases} -\alpha c(1,t), & \beta \ll 1, \quad (15) \\ -\dfrac{\alpha}{\beta}, & \beta \gg 1. \quad (16) \end{cases}$$

Solving (12) subject to (13) and (14) gives

$$\bar{c}(x,s) = a(s)\cosh(\sqrt{s}x) + \frac{1}{s}. \tag{17}$$

and taking the inverse Laplace transform yields

$$c(x,t) = 1 + \mathcal{L}^{-1}\left\{a(s)\cosh(\sqrt{s}x)\right\}. \tag{18}$$

We may now apply (15) and (16) in turn to obtain small and large β solutions.

Small β solution. Here, we obtain $a(s)$ by differentiating (17) with respect to x and applying the Laplace transform of (15):

$$a(s) = -\frac{\alpha}{s\left[\sqrt{s}\sinh(\sqrt{s}) + \alpha\cos(\sqrt{s})\right]}.$$

Then, from (18), it follows that

$$c(x,t) = 1 - \alpha\mathcal{L}^{-1}\left\{\frac{\cosh(\sqrt{s}x)}{s\left[\sqrt{s}\sinh(\sqrt{s}) + \alpha\cosh(\sqrt{s})\right]}\right\}. \tag{19}$$

It may readily be shown that no branch points exist, so the residue theorem is used to evaluate the inverse Laplace transform. The poles are given by

$$s = 0 \quad \text{and} \quad \sqrt{s}\sinh(\sqrt{s}) + \alpha\cosh(\sqrt{s}) = 0,$$

and, for convenience, setting $\sqrt{s} = i\chi$ in the transcendental equation gives

$$\chi \sin(\chi) - \alpha \cos(\chi) = 0. \tag{20}$$

Hence there is a simple pole at $s = 0$ and infinitely many simple poles at $s_n = -\chi_n^2$ for $n \in \mathbb{N}$, where χ_n are the roots of (20). After a trivial calculation, it is clear that

$$\operatorname*{Res}_{s=0} = \frac{1}{\alpha},$$

and, using L'Hôpital's rule, the residue at $s = s_n$ is given by

$$\operatorname*{Res}_{s=s_n} = -\frac{2\cos(\chi_n x)}{\chi_n\big[\chi_n \cos(\chi_n) + (\alpha+1)\sin(\chi_n)\big]} e^{-\chi_n^2 t}.$$

Then, applying the residue theorem, it follows from (19) that

$$c(x,t) = \sum_{n=1}^{\infty} \frac{2\alpha\cos(\chi_n x)}{\chi_n\big[\chi_n \cos(\chi_n) + (\alpha+1)\sin(\chi_n)\big]} e^{-\chi_n^2 t}.$$

Re-arranging (20) to obtain

$$\alpha\cos(\chi_n) = \chi_n \sin(\chi_n),$$

and choosing $x = 1$ results in

$$c(1,t) = \sum_{n=1}^{\infty} \frac{2\sin(\chi_n)}{\chi_n \cos(\chi_n) + (\alpha+1)\sin(\chi_n)} e^{-\chi_n^2 t},$$

i.e. the small β solution (4.7), to leading-order.

Large β solution. Here, we obtain $a(s)$ by differentiating (17) with respect to x and applying the Laplace transform of (16):

$$a(s) = -\frac{\alpha}{\beta\big[s^{3/2}\sinh(\sqrt{s})\big]}.$$

Then, from (18), it follows that

$$c(x,t) = 1 - \frac{\alpha}{\beta}\mathcal{L}^{-1}\left\{\frac{\cosh(\sqrt{s}x)}{s^{3/2}\sinh(\sqrt{s})}\right\}. \tag{21}$$

It may readily be shown that no branch points exist, so the residue theorem is used to evaluate the inverse Laplace transform. The poles are given by

$$s = 0 \quad \text{and} \quad \sinh(\sqrt{s}) = 0,$$

i.e. there is a pole of order 2 at $s = 0$ and infinitely many simple poles at $s_n = -n^2\pi^2$ for $n \in \mathbb{N}$. Using L'Hôpital's rule to calculate the residues gives

$$\operatorname*{Res}_{s=0} = \frac{x^2}{2} + t - \frac{1}{6},$$
$$\operatorname*{Res}_{s=s_n} = \frac{2\cos(n\pi x)}{(-1)^{n+1}n^2\pi^2} e^{-n^2\pi^2 t}.$$

Then, applying the residue theorem, it follows from (21) that

$$c(x,t) = 1 - \frac{\alpha}{\beta}\left(\frac{x^2}{2} + t - \frac{1}{6} + 2\sum_{n=1}^{\infty} \frac{\cos(n\pi x)}{(-1)^{n+1}n^2\pi^2} e^{-n^2\pi^2 t}\right).$$

Choosing $x = 1$ and noting that $\cos(n\pi) = (-1)^n$ results in

$$c(1,t) = 1 - \frac{\alpha}{\beta}\left(t + \frac{1}{3} - 2\sum_{n=1}^{\infty} \frac{1}{n^2\pi^2} e^{-n^2\pi^2 t}\right),$$

i.e. the large β solution (4.11), to first-order.

Numerical method for solving (3.5)

Product integration methods are applied to derive an implicit numerical scheme for solving (3.5), given by

$$c(1,t) = 1 - \alpha \int_0^t \sum_{n=1}^{\infty} \sigma_n e^{-\gamma_n^2(t-\tau)} \frac{c(1,\tau)}{1 + \beta c(1,\tau)}\, d\tau,$$

where σ_n is a constant defined as

$$\sigma_n = \frac{2\big[\gamma_n \cos(\gamma_n) + \mu \sin(\gamma_n)\big]}{\gamma_n \cos(\gamma_n) + (\mu + 1)\sin(\gamma_n)}.$$

Replacing t by $t_i = i\Delta t$, where $i = 1, 2, \ldots, T$ such that $T\Delta t$ is the final time of interest, the integral can be written as a sum of integrals over smaller intervals:

$$c(1,t_i) = 1 - \alpha \sum_{j=0}^{i-1} \int_{t_j}^{t_{j+1}} \sum_{n=1}^{\infty} \sigma_n e^{-\gamma_n^2(t_i-\tau)} \frac{c(1,\tau)}{1 + \beta c(1,\tau)}\, d\tau.$$

This can be re-written as

$$c(1,t_i) \approx 1 - \alpha \sum_{j=0}^{i-1} \left(\int_{t_j}^{t_{j+1}} \sum_{n=1}^{\infty} \sigma_n e^{-\gamma_n^2(t_i-\tau)}\, d\tau\right) \frac{c(1,t_{j+1})}{1 + \beta c(1,t_{j+1})},$$

assuming the following approximation over $[t_j, t_{j+1}]$:

$$\frac{c(1,\tau)}{1+\beta c(1,\tau)} \approx \frac{c(1,t_{j+1})}{1+\beta c(1,t_{j+1})}.$$

Now, performing the integration with $t_j = j\Delta t$ gives

$$\int_{t_j}^{t_{j+1}} \sum_{n=1}^{\infty} \sigma_n e^{-\gamma_n^2(t_i-\tau)}\, d\tau = \sum_{n=1}^{\infty} \frac{\sigma_n}{\gamma_n^2}\left(e^{-\gamma_n^2\Delta t(i-j-1)} - e^{-\gamma_n^2\Delta t(i-j)}\right),$$

and so

$$c(1,t_i) \approx 1 - \alpha \sum_{j=0}^{i-1}\left[\sum_{n=1}^{\infty} \frac{\sigma_n}{\gamma_n^2}\left(e^{-\gamma_n^2\Delta t(i-j-1)} - e^{-\gamma_n^2\Delta t(i-j)}\right)\right] \frac{c(1,t_{j+1})}{1+\beta c(1,t_{j+1})}.$$

It is noted that

$$\begin{aligned}
&\sum_{j=0}^{i-1}\left[\sum_{n=1}^{\infty} \frac{\sigma_n}{\gamma_n^2}\left(e^{-\gamma_n^2\Delta t(i-j-1)} - e^{-\gamma_n^2\Delta t(i-j)}\right)\right] \frac{c(1,t_{j+1})}{1+\beta c(1,t_{j+1})} \\
&= \left[\sum_{n=1}^{\infty} \frac{\sigma_n}{\gamma_n^2}\left(1 - e^{-\gamma_n^2\Delta t}\right)\right] \frac{c(1,t_i)}{1+\beta c(1,t_i)} \\
&\quad + \sum_{j=0}^{i-2}\left[\sum_{n=1}^{\infty} \frac{\sigma_n}{\gamma_n^2}\left(e^{-\gamma_n^2\Delta t(i-j-1)} - e^{-\gamma_n^2\Delta t(i-j)}\right)\right] \frac{c(1,t_{j+1})}{1+\beta c(1,t_{j+1})},
\end{aligned}$$

so an approximation to $c(1,t_i)$ may be obtained by finding the roots, c_i, of the following implicit equation:

$$\begin{aligned}
&c_i + \alpha\left[\sum_{n=1}^{\infty} \frac{\sigma_n}{\gamma_n^2}\left(1 - e^{-\gamma_n^2\Delta t}\right)\right] \frac{c_i}{1+\beta c_i} \\
&= 1 - \alpha \sum_{j=0}^{i-2}\left[\sum_{n=1}^{\infty} \frac{\sigma_n}{\gamma_n^2}\left(e^{-\gamma_n^2\Delta t(i-j-1)} - e^{-\gamma_n^2\Delta t(i-j)}\right)\right] \frac{c_{j+1}}{1+\beta c_{j+1}}.
\end{aligned}$$

Numerical method for solving (3.6)

Similarly, product integration methods are applied to derive an implicit numerical scheme for solving (3.6), given by

$$c(1,t) = 1 - \alpha \int_0^t k_0(1,t-\tau)\frac{c(1,\tau)}{1+\beta c(1,\tau)}\, d\tau,$$

where

$$k_0(1,t) = 1 + 2\sum_{n=1}^{\infty} e^{-n^2\pi^2 t}.$$

For the following derivation, $k_0(1,t)$ is re-written as

$$k_0(1,t) = \frac{1}{\sqrt{\pi t}}\left(1 + 2\sum_{n=1}^{\infty} e^{-n^2/t}\right),$$

using result (5) in [1]. Using this form for $k_0(1,t)$, (3.6) becomes

$$c(1,t) = 1 - \frac{\alpha}{\sqrt{\pi}}\int_0^t \frac{1}{\sqrt{t-\tau}}\left(1 + 2\sum_{n=1}^{\infty} e^{-n^2/(t-\tau)}\right)\frac{c(1,\tau)}{1+\beta c(1,\tau)}\,d\tau.$$

Replacing t by $t_i = i\Delta t$, where $i = 1, 2, \ldots, T$ such that $T\Delta t$ is the final time of interest, the integral can be re-written as a sum of integrals over smaller intervals:

$$c(1,t_i) = 1 - \frac{\alpha}{\sqrt{\pi}}\sum_{j=0}^{i-1}\int_{t_j}^{t_{j+1}} \frac{1}{\sqrt{t_i-\tau}}\left(1 + 2\sum_{n=1}^{\infty} e^{-n^2/(t_i-\tau)}\right)\frac{c(1,\tau)}{1+\beta c(1,\tau)}\,d\tau.$$

This can be re-written as

$$c(1,t_i) \approx 1 - \frac{\alpha}{\sqrt{\pi}}\sum_{j=0}^{i-1}\left(\int_{t_j}^{t_{j+1}} \frac{1}{\sqrt{t_i-\tau}}\,d\tau\right)\left(1 + 2\sum_{n=1}^{\infty} e^{-n^2/(t_i-t_{j+1})}\right)\frac{c(1,t_{j+1})}{1+\beta c(1,t_{j+1})},$$

assuming the following approximation over $[t_j, t_{j+1}]$:

$$\left(1 + 2\sum_{n=1}^{\infty} e^{-n^2/(t-\tau)}\right)\frac{c(1,\tau)}{1+\beta c(1,\tau)} \approx \left(1 + 2\sum_{n=1}^{\infty} e^{-n^2/(t-t_{j+1})}\right)\frac{c(1,t_{j+1})}{1+\beta c(1,t_{j+1})}$$

Performing the integration with $t_j = j\Delta t$ gives

$$\int_{t_j}^{t_{j+1}} \frac{1}{\sqrt{t_i-\tau}}\,d\tau = 2\sqrt{\Delta t}\left(\sqrt{i-j} - \sqrt{i-j-1}\right),$$

and so

$$c(1,t_i) \approx 1 - \frac{2\alpha\sqrt{\Delta t}}{\sqrt{\pi}}\sum_{j=0}^{i-1}\left(\sqrt{i-j} - \sqrt{i-j-1}\right)\left(1 + 2\sum_{n=1}^{\infty} e^{-n^2/(t_i-t_{j+1})}\right)\frac{c(1,t_{j+1})}{1+\beta c(1,t_{j+1})}.$$

It is noted that

$$\sum_{j=0}^{i-1}\left(\sqrt{i-j}-\sqrt{i-j-1}\right)\left(1+2\sum_{n=1}^{\infty}e^{-n^2/(t_i-t_{j+1})}\right)\frac{c(1,t_{j+1})}{1+\beta c(1,t_{j+1})}$$
$$=\frac{c(1,t_i)}{1+\beta c(1,t_i)}+\sum_{j=0}^{i-2}\left(\sqrt{i-j}-\sqrt{i-j-1}\right)\left(1+2\sum_{n=1}^{\infty}e^{-n^2/(t_i-t_{j+1})}\right)\frac{c(1,t_{j+1})}{1+\beta c(1,t_{j+1})},$$

so an approximation to $c(1,t_i)$ may be obtained by finding the roots, c_i, of the following implicit equation:

$$c_i+\frac{2\alpha\sqrt{\Delta t}}{\sqrt{\pi}}\frac{c_i}{1+\beta c_i}$$
$$=1-\frac{2\alpha\sqrt{\Delta t}}{\sqrt{\pi}}\sum_{j=0}^{i-2}\left(\sqrt{i-j}-\sqrt{i-j-1}\right)\left(1+2\sum_{n=1}^{\infty}e^{-n^2/(t_i-t_{j+1})}\right)\frac{c_{j+1}}{1+\beta c_{j+1}}.$$

Numerical method for solving (4.3)

An explicit Euler numerical scheme is derived for solving (4.3), given by

$$c_1(1,t)=-\alpha\int_0^t k(1,t-\tau)\big[c_1(1,\tau)-c_0(1,\tau)^2\big]\,d\tau,$$

where

$$c_0(1,t)=\frac{\mu}{\alpha\mu+\alpha+\mu}+\sum_{n=1}^{\infty}\frac{2\big[\mu\cos(\lambda_n)-\lambda_n\sin(\lambda_n)\big]e^{-\lambda_n^2 t}}{(\alpha\mu+\alpha+\mu-\lambda_n^2)\cos(\lambda_n)-\lambda_n(2+\alpha+\mu)\sin(\lambda_n)},$$

and λ_n are the roots of

$$(\alpha\mu-\lambda^2)\sin(\lambda)+\lambda(\alpha+\mu)\cos(\lambda)=0.$$

Replacing t by $t_i=i\Delta t$, where $i=1,2,\ldots,T$ such that $T\Delta t$ is the final time of interest, the integral can be re-written as a sum of integrals over smaller intervals:

$$c_1(1,t_i)=-\alpha\sum_{j=0}^{i-1}\int_{t_j}^{t_{j+1}}k(1,t_i-\tau)\big[c_1(1,\tau)-c_0(1,\tau)^2\big]\,d\tau.$$

Then, using the argument of Riemann sums gives

$$c_1(1,t_i)\approx-\alpha\Delta t\sum_{j=0}^{i-1}k(1,t_i-t_j)\big[c_1(1,t_j)-c_0(1,t_j)^2\big].$$

Thus, an approximation to $c_1(1,t_i)$ may be obtained by finding the roots, $c_{1,i}$, of the following explicit equation:

$$c_{1,i} = -\alpha\Delta t \sum_{j=0}^{i-1} k(1, t_i - t_j)\big[c_{1,j} - c_{0,j}^2\big].$$

Similarly, an explicit Euler numerical scheme can be used to obtain $c_1(1,t)$ for the case when $\mu = 0$, given by

$$c_1(1,t) = -\alpha \int_0^t k_0(1, t-\tau)\big[c_1(1,\tau) - c_0(1,\tau)^2\big]\, d\tau,$$

where

$$c_0(1,t) = \sum_{n=1}^{\infty} \frac{2\sin(\chi_n)e^{-\chi_n^2 t}}{\chi_n\cos(\chi_n) + (\alpha+1)\sin(\chi_n)},$$

and χ_n are the roots of

$$\chi\sin(\chi) - \alpha\cos(\chi) = 0.$$

As before, the integral can be re-written as a sum of integrals over smaller intervals, then using the argument of Riemann sums gives

$$c_1(1,t_i) \approx -\alpha\Delta t \sum_{j=0}^{i-1} k_0(1, t_i - t_j)\big[c_1(1,t_j) - c_0(1,t_j)^2\big].$$

Thus, for the case when $\mu = 0$, an approximation to $c_1(1,t_i)$ may be obtained by finding the roots, $c_{1,i}$, of the following explicit equation:

$$c_{1,i} = -\alpha\Delta t \sum_{j=0}^{i-1} k_0(1, t_i - t_j)\big[c_{1,j} - c_{0,j}^2\big].$$

References

[1] B. Jumarhon, S. McKee, and T. Tang. The proof of an inequality arising in a reaction-diffusion study in a small cell. *J Comp App Math*, 51:99-101, 1994. doi:10.1016/03770427(94)90092-2.